Designed Single-Step Synthesis, Structure, and Derivative Textural Properties of Well-Ordered Layered Penta-Coordinate Silicon Alcoholate Complexes

Xiansen Li,*[a] Vladimir K. Michaelis,[b,c] Ta-Chung Ong,[b,c] Stacey J. Smith,[b] Robert G. Griffin,[b,c] and Evelyn N. Wang*[a]

[a] Dr. X. Li, Prof. E. N. Wang, Department of Mechanical Engineering, Massachusetts Institute of Technology, 77 Massachusetts Ave., Cambridge, MA 02139, (USA)
E-mail: xsli@mit.edu; enwang@mit.edu.
[b] Dr. V. K. Michaelis, T.-C. Ong, Dr. S. J. Smith, Prof. R. G. Griffin, Department of Chemistry, Massachusetts Institute of Technology, 77 Massachusetts Ave., Cambridge, MA 02139, (USA).
[c] Dr. V. K. Michaelis, T.-C. Ong, Prof. R. G. Griffin, Francis Bitter Magnet Laboratory, Massachusetts Institute of Technology, 77 Massachusetts Ave., Cambridge, MA 02139, (USA).

Abstract: The controllable synthesis of well-ordered layered materials with specific nanoarchitecture poses a grand challenge in materials chemistry. We report the solvothermal synthesis of two structurally analogous 5-coordinate organosilicate complexes via a novel transesterification mechanism. Since the polycrystalline nature of the intrinsic hypervalent Si complex thwarts the endeavor in determining its structure, a novel strategy concerning the elegant addition of a small fraction of B species as an effective crystal growth mediator and a sacrificial agent is proposed to directly prepare diffraction-quality single crystals without disrupting the intrinsic elemental type. In the determined crystal structure, two monomeric primary building units (PBUs) self-assemble into a dimeric asymmetric secondary BU via strong Na^+-O^{2-} ionic bonds. The designed one-pot synthesis is straightforward, robust, and efficient, leading to a well-ordered (10ī)-parallel layered Si complex with its principal interlayers intercalated with extensive van der Waals gaps in spite of the presence of substantial Na^+ counter-ions as a result of unique atomic arrangement in its structure. On the other hand, upon fast pyrolysis, followed by acid leaching, both complexes are converted into two SiO_2 composites bearing BET surface areas of 163.3 and 254.7 m^2 g^{-1} for the pyrolyzed intrinsic and B-assisted Si complexes, respectively. The transesterification methodology merely involving alcoholysis but without any hydrolysis side reaction is designed to have generalized applicability for use in synthesizing new layered metal-organic compounds with tailored PBUs and corresponding metal oxide particles with hierarchical porosity.

Keywords: boron-mediated synthesis • hypervalent compounds • layered compounds • modified transesterification • van der Waals gap

Introduction

In contrast to the ubiquitous tetrahedrally coordinated silicate species, the reports of 5-coordinate Si ([5]Si) species have so far been infrequent in alkoxide-based crystalline solids.[1-6] Consequently, there are still some unknown aspects about their physicochemical properties. The laborious preparations of several [5]Si complexes were disclosed in multiple synthetic steps[1,3] by reacting SiO_2 grains with alkali hydroxide in excessive ethylene glycol (EG) solvent with continuous distillation of EG and coincident distillative removal of liberated water to drive the dissolution process to proceed smoothly. Additionally, this technique encountered severe foaming in the presence of Na^+ cations over the course of the synthetic process. More importantly, water-sensitive or hygroscopic silicoalcoholate complexes cannot be produced by this method due to the unavoidable water interference therein. Although the conventional transesterification reaction involving carboxylic acid esters has already been well-exploited in organic synthesis, e.g., biodiesel production from triglyceride and light alcohols,[7] it is not applicable for the preparation of metal-organic compounds (e.g., layered 5-coordinate organosilicates) without any modification of the reaction.

Crystallography and NMR are the most powerful techniques available for unraveling unknown molecular structures. However, neither polycrystalline powders nor single crystals of 5-coordinate alkoxysilicates with mixed methanolate/glycolate ligands have been thus far disclosed, not to mention their crystal structure determination[1,3a]. In general, growing large single crystals indispensable for crystallography can be classified into two major categories: direct and indirect methods. In the latter case, it manages to transform the polycrystalline powders into the respective single crystals by time-intensive recrystallization techniques provoked primarily by controlled solvent evaporation, slow cooling, vapor diffusion, liquid-liquid inter-diffusion, sublimation, and convection, *etc*. Another disadvantage associated with the indirect method is that the recrystallized single crystals are occasionally phase transformed.[8] Particularly, the effective preparations of crystallographically resolvable single crystals are a significant challenge for Si-containing compounds owing to the strong propensity of silicates towards fast gelation even at the reactant mixing stage. As a general countermeasure against the undesirable gelling, excessive strong chelators and/or sparingly soluble silica sources, e.g., quartz, are admixed together with dilute alkaline solutions to regulate the relative contribution between nucleation and crystal growth,[9-11] thereby causing dramatically extended synthetic duration and aggravated waste disposal loads.

The versatility of well-ordered layered materials makes them quite attractive for several important applications including lithium-ion batteries,[12] supercapacitors,[13] drug delivery,[14] adsorbents,[15,16] catalysts,[17] and catalyst supports.[18] Among the known layered materials, those with their interlayers intimately linked together only by long-range attractive force of van der Waals type (i.e., so-called van der Waals gap as typically found in the FeOCl[12a] and TiS_2[12c]) are quite rare in the presence of charge-

balancing alkali metal counter-ions. This feature could be quite useful for advanced lubricants and precursors towards preparing nanoflake/polymer composite membranes for gas-/liquid-mixtures separations.

In this contribution, we report a novel single-step solvothermal preparative methodology, i.e., a modified transesterification mechanism, for preparing two layered [5]Si complexes with a similar asymmetric unit. In addition, a new B-mediated approach that does not involve any B incorporation into the intrinsic host silicate matrix is formulated herein for the facile synthesis of large-sized single crystals of the hitherto poorly-characterized binary-ligand [5]Si complex, with which its crystal structure is for the first time determined in this study. Also, we demonstrate a proof-of-concept study regarding the rapid pyrolytic conversion of these Si complex precursors into high-surface-area amorphous SiO_2 composites with minor residual carbon loadings.

Results and Discussion

Solvothermal synthesis: A modified transesterification strategy using pseudo-covalent metal alkoxide ester instead of the traditional carboxylic acid ester is proposed for the one-pot synthesis of two well-ordered layered [5]Si complexes under anhydrous circumstances. Over the course of solvothermal reaction involving B mediator, the effective deprotonation of EG reactant (only 1.5-fold excess from stoichiometry) is initially accomplished by the operative strong base catalyst of excessive sodium methoxide to initiate the S_N2 nucleophilic substitution reaction, leading to the formation of ethylene glycolate anions. These incoming anions thus formed then compete with stoichiometric amounts of methanolates for nucleophilic attack of the Si electrophiles, thereby causing the concurrent departure of CH_3O^- anions from $Si(OCH_3)_4$ reactant. Due to the chelating nature of the bidentate glycolate, Si electrophile obviously possesses a coordinative preference for glycolate over monodentate methanolate, thus affording a unique [5]Si complex at an ultimate methanolate/glycolate ratio of 1:2 in the empirical formula of the B-assisted Si complex (Table S1). The designed transesterification mechanism is advantageous because it only involves alcoholysis but precludes any hydrolysis side-reaction, thereby effectively eliminating the coincident generation of metal hydroxide precipitate as a contaminant. It also offers the opportunity and flexibility for designing novel moisture-sensitive or hygroscopic compounds.

It is worth noting that initial studies were dedicated to detailed characterization of the intrinsic [5]Si complex without any B pre-dosing. However, this attempt was thwarted by the failure in directly achieving X-ray quality single crystals. Inspired by the intriguing borosilicate glass and zeolite chemistries,[19-21] where B heteroatom shows the difficulty in isomorphously inserting in considerable proportion into the silicate network matrix due to the substantial mismatching between d(Si-O) (1.58-1.64 Å)[22] and d(B-O) (1.44-1.52 Å) both in 4-coordinate geometries,[23] an efficient strategy, by which

crystallographically resolvable single crystals are successfully achieved by taking advantage of B-mediated transesterification synthesis, is developed herein in order to address the hitherto unknown crystal structure of the [5]Si complex bearing mixed alcoholates. It is found that $B(OCH_3)_3$ additive allows for a well-mobile thin gel precursor formulation rather than the instantaneous creation of an undesirable sluggish thick gel entity in the absence of B mediator. In this case, the vast majority of B species are supposed to still partition in the dynamically equilibrated bulk solution in close contact with the gel phase. The dynamic bi-phasic B distribution effectively inhibits diverse Si species from full condensation into a thick gel mass that is detrimental for large single crystal growth. It is well-known that B forms diester complexes with polyol chelators more readily than does Si. It therefore seems likely that organosilicate crystal growth is seeded by rapidly created bis(glycolato)borate crystal nuclei. When the crystallization process progresses, B would be gradually expelled from the growing crystal lattice because it cannot support 5-coordination unlike Si. The hypothetical [5]B species isomorphously substituting for [5]Si sites is highly energetically unfavorable due to the large negative charge density (i.e., [5]B^{2-}) localized on the small B center, preliminarily validating the lack of detectable B insertion into the 5-coordinate organosilicate matrix. Hence, this B-mediated synthetic methodology proposed here provides a unique opportunity to study in depth Si chemistry by rationally growing the relevant single crystals.

PXRD analysis: Experimental powder X-ray diffraction (PXRD) patterns of the intrinsic Si complex (A), B-assisted counterpart (B), and simulated PXRD pattern of a single crystal of the latter (C) are graphically stacked in Figure 1. Both samples are highly crystalline, as evidenced by negligible background intensities and very sharp major peaks. The zoomed-in profiles in the high-angle regime (Figure S1 A and B) reveal that following B dosing (5.3% relative to Si), the XRD pattern differs to some extent from that of the intrinsic Si complex in terms of peak *2θ* position and relative intensity. Interestingly, regardless of the preparative methodology, the intrinsic Si complex exhibits the XRD pattern analogous to those reported in Refs.[2,3] for $Na_2Si_2(OCH_2CH_2O)_5$ complex but with the most intense peak shifting from 11.02° *2θ* for the former down to 10.81° *2θ* for the latter, presumably originating from the swelling effect of EG solvent adopted in the latter syntheses. Namely, they are isostructural with each other. Combining B and C in both Figures 1 and S1, the experimental PXRD pattern of the B-assisted Si complex closely matches the simulated pattern derived from the single-crystal XRD (SCXRD) structure, manifesting the high phase purity of the well-developed single crystalline grains. The strongest peak corresponding to (10ī) reflection at 11.27° *2θ* (7.84 Å in interplanar *d*-spacing) is indicative of a well-organized layered B-assisted Si complex with its dominant interlayers parallel to the (10ī) plane (Figure 1 B).

After rapid pyrolysis of both Si complexes at 800 °C for 8-10 min, the resultant samples of Si_py and Si+B_py are proven X-ray amorphous, regardless of B dosing (data not shown).

SCXRD, ^{29}Si and ^{13}C MAS NMR analyses: The molecular geometry and atom-labeling scheme for

the B-assisted Si complex are illustrated in the thermal ellipsoid plot of Figure 2. The complex crystallizes in the monoclinic crystal system and the space group $P2_1/n$ (Table S1) with the asymmetric unit containing one dimeric sodium tetrakis(glycolato)bis(methanolato)silicate complex $Na_2Si_2(OCH_3)_2(OCH_2CH_2O)_4$. Both Si centers are uniquely 5-coordinate; each is bound by two bidentate glycolate chelators and one monodentate methanolate ligand. ^{29}Si magic angle spinning nuclear magnetic resonance (MAS NMR) (Figure 3 A) reveals two distinct [5]Si resonances located at -105 and -108 ppm further supporting the assignment of two crystallographic Si sites.[2,3a,4] The ^{13}C{^{1}H} MAS NMR spectrum (Figure 3 B) shows two well-resolved regions which can be assigned to the ethylene glycolate (63 ppm) and methanolate (53 ppm) ligands.[24] The carbon ratio between the glycolate and methanolate sites using both direct excitation and cross polarization (CP) gives *ca.* 4:1, corroborating the monomeric BU structure determined by SCXRD studies. Since the carbon atoms (C5 and C6) of one of the four glycolates are position-disordered, we speculate the disorder of the glycolates is the cause of the extra shoulder resonances observed in the ^{13}C MAS NMR spectrum (i.e., 66 and 54 ppm in Figure 3 B). Similarly, two discernible regions are also observed in the ^{13}C{^{1}H} MAS NMR spectrum of the B-undoped Si complex $Na_2Si_2(OCH_2CH_2O)_5$ (Figure 3 C) with the least intense resonance at 52.5 ppm probably attributable to a very small number of the unbound MeOH solvent molecules tightly occluded in the interplanar voids, as found in Ref.[24]. There remain three resolvable resonances in the bound glycolate domain with an intensity ratio of *ca.* 1:2:2. Among them, the weakest resonance is assigned to the sole bridging glycolate ligand with the other two resonances corresponding to the remaining four glycolate chelators. The position-disordered carbon atoms of glycolates like C5 and C6 in Figure 2 may account for the resonance splitting of these four glycolates situated in a locally similar chemical environment.

As shown in Figure 2, concerning one monomeric BU $NaSi(OCH_3)(OCH_2CH_2O)_2$, the central [5]Si1 atom exclusively adopts an quasi-trigonal-bipyramidal geometry. Oxygens O1 and O3 occupy the axial positions and form the elongated Si1-O bonds of 1.7656(10) and 1.7422(10) Å, respectively.[32] Oxygens O2, O4, and O9 take up the equatorial positions at a little shorter Si1-O bond lengths of 1.695(10), 1.6858(10), and 1.6762 (10) Å, respectively. On the basis of the respective atomic coordinates,[32] it is calculated that the Si1 center resides 0.051 Å below the plane defined by O2, O4, and O9 in reference to the O1 apex. These bond lengths are in close proximity to the Si-O bond distances found in Refs.,[3,25] where [5]Si complexes with their atomic structures different from this study were reported, but slightly longer than d(Si-O) of 1.59-1.64 Å for [SiO_4] tetrahedra contained in zeolites.[26,27] Partially arising from inherently asymmetric stereo-configuration of mixed alkoxy ligands, distortions from the idealized trigonal-bipyramidal geometry towards a square pyramid with O9 at the apex are conceivable, as has been found for other [5]Si compounds. On the other hand, there exist six Na-O contacts in the 2.3032(11)-2.4106(11) Å scope definitely contributing more or less to such distortions.

Packing plots of the B-assisted Si complex viewed along the crystallographic *b* and [101] axes are provided in Figure 4 A and B, respectively. By coupling both figures, it can be envisaged that the 3D crystal structure is constructed of periodically aligned layers parallel to (10ī) plane instead of parallel chain-like BUs, which agrees well with the above PXRD results. Interestingly, both Si and Na atoms are in-plane with the layers with their peripherals decorated with the arrays of methanolates and glycolates, resulting in the interlayers uniquely held together by extensive van der Waals attractive force. The weak interaction of this type may readily bring about the interplanar slip. In-plane Na^+ ions behave both as charge-counterbalancing cations and cross-linkers, strongly tethering the monomers in each layer together by strong Na^+-O^{2-} ionic bonding interactions. Due to full condensation of the EGs catalyzed by $NaOCH_3$, the absence of free hydroxyl groups in its structure interprets the lack of identifiable hydrogen bonding interactions on inter-atoms in the entire crystal lattice.

^{11}B MAS NMR analysis: SCXRD analysis shows no evidence of B heteroatom incorporation within the crystal lattice of the B-assisted Si complex. However, one single crystal may not be representative of the entire sample. Its bulk powders is thus qualitatively analyzed via ^{11}B MAS NMR (data not shown) in light of the inherent sensitivity for detecting [11]B chemical environments due to its high natural abundance (80.1%). No detectable B species are identified, suggesting the B content is << 1 wt%,[28,29] if any.

ATR-FTIR spectroscopy: Attenuated total reflectance-Fourier transform infrared (ATR-FTIR) spectra of the B-undoped sample (A), B-assisted one without (B) and with (C) exposure to air for 10 min are presented in Figure 5. For the B-undoped polycrystalline powders, a broad band at 3000-3600 cm^{-1} attributable to hydroxyl absorption signal (Figure 5 A) is a combined result of physisorbed moisture and encapsulated MeOH solvent residues, as corroborated by ^{13}C MAS NMR (Figure 3 C). In contrast, this weak broad band is significantly enhanced in intensity even subjecting to ambient exposure for 10 min (Figure 5 B and C), highlighting strong hygroscopicity of the B-assisted Si single crystals. As shown in Figure 5 A and B, the absorption band at 2750-2980 cm^{-1} is assigned to the sp^3 C-H bond stretching vibrations, whereas the band at 1340-1500 cm^{-1} corresponds to the C-H bond bending vibrations. More specifically, two discernible peaks at 2870/2950 cm^{-1} (methyl C-H symmetrical/asymmetrical stretching vibrations) confirm the existence of methyl groups within both Si complexes but with the methyl origin differing from each other (residual MeOH solvents for the intrinsic sample vs. methanolate ligands for the B-assisted one). Strong Si-O-C bond stretching vibrations at 933-1110 cm^{-1} are observed in both samples, in which the 1030-1070 cm^{-1} absorption band originating from the C-O bond stretching vibrations dominates the above spectral range. The absorption band at 600-900 cm^{-1} is attributed to varying Si-O bond vibrations including O-Si-O bond vibrational frequency.[30] Any distinguishable peak at *ca.* 670 cm^{-1} corresponding to the O-B-O bond bending vibrations[31] does not appear in the B-assisted Si complex (Figure 5 B and C), revealing the B content below the detection limit of IR spectroscopy.

EA: Bulk elemental analysis (EA) is conducted to quantitatively determine the final whereabouts of the B species. Table 1 tabulates the elemental composition of both Si complexes along with the refined SCXRD empirical formula for comparison sake. Based upon earlier PXRD and ^{13}C MAS NMR analyses, $Na_2Si_2(OCH_2CH_2O)_5$ formula is assigned to the B-undoped Si complex, which is qualitatively in accord with the apparent composition of $Na_{1.94}Si_2C_{9.80}H_{21.44}O_{10.82}$. In view of the deliquescence-prone nature of the B-assisted sample (Figures 5 and 6), the drying step preceding EA is supposed to drive off a small number of hydrolytically produced MeOH and physisorbed moisture, thus resulting in a slight underestimation of both carbon and hydrogen contents in relation to SCXRD result. On the other hand, the finding that the B content is too low to be accurately quantified provides the most direct evidence, lending further support to the conclusion that the B-assisted Si complex is devoid of identifiable B incorporation.

TG and DTG analyses: The thermal stabilities of both Si complexes are evaluated by thermogravimetric (TG) technique both operating in flowing N_2 streams, as illustrated in Figure 6. For the B-undoped polycrystalline powders, between 30 and 370 °C, there exists a minor weight loss (1.2%) likely corresponding to the evaporation of physisorbed water and residual MeOH solvents. With increasing temperature, one pronounced weight loss is observed before the final plateau. A dramatic weight loss associated with the framework collapse is observable over 370-550 °C with a temperature inflection point at 430 °C. In comparison with the theoretical overall weight loss of 56.4%, the corresponding value of 53.8% is experimentally obtained while ramping the temperature from RT to 800 °C in an anaerobic environment, ultimately leaving behind the blackened end powders of decomposition. Namely, after pyrolysis a residual carbon loading of *ca.* 2.6% for the Si_py composite is theoretically predicted.

In contrast, the onset degradation temperature of the B-assisted single crystals occurs at 320 °C with a total weight loss of 2.8% from RT to 320 °C. A larger weight loss is responsible for stronger hygroscopicity of the B-assisted Si complex relative to the undoped counterpart. In the entire temperature range, a total weight loss of 52.0% is measured. The theoretical weight loss for the conversion from $Na_2Si_2C_{10}H_{22}O_{10}$ to an oxide of stoichiometry $Na_2O·2SiO_2$ is 54.9%, which means that the Si+B_py composite theoretically contains a carbon loading of approximately 2.9%. Both materials are hence quite thermally stable under inert gas atmospheres.

SEM observations: Figures 7 and 8, respectively, show the SEM images of Si_py, Si_py_al, Si+B_py, and Si+B_py_al, as well as the corresponding magnified images of one single grain in the insets. SEM images of the intrinsic silica composite (Figure 7 A) indicates that the unwashed sample is composed of some large irregular grains with a wide particle size distribution. The magnified image (inset) reveals that the large secondary grain consists of the aggregation of numerous small primary spherical particles (*ca.* 3.4 μm in mean diameter) and interspersed micro-lamellas, which are tightly held together by the

thermally induced sodium silicate binder. After acid leaching, the secondary grains are broken up into smaller irregular pieces as a result of the dissolution of the binder (Figure 7 B). In contrast, the unwashed secondary particles of Si+B_py are more uniform and smaller (Figure 8 A) together with the primary spheres of roughly 1.2 μm in average grain diameter (inset in Figure 8 A). Notably, despite the wide dispersity of particle sizes, a portion of silica nanoparticles are successfully achieved upon experiencing simple acid-leaching treatment (Figure 8 B).

Gas sorption analyses on the pyrolyzed products: Figures 9 and 10, respectively, show the N_2 sorption isotherms of Si_py, Si_py_al, Si+B_py, and Si+B_py_al, as well as their corresponding PSDs (insets). Textural parameters for both sets of amorphous silica composite materials are summarized in Table 2. As seen in both figures, all samples except for Si+B_py exhibit Type IV isotherms with widespread yet distinct hysteresis loops of Type H3 in the IUPAC classification, characteristic of mesoporous materials with relatively broad PSDs that are also reflected by the respective PSDs (insets in Figures 9 and 10). It is found that the sorption isotherms give dramatic increases in S_{BET} from 35.5 for Si_py to 163.3 m^2 g^{-1} for Si_py_al, and from 30.0 for Si+B_py to 254.7 m^2 g^{-1} for Si+B_py_al. The corresponding total pore volumes of these four composites are respectively 0.051, 0.211, 0.046 and 0.302 ml g^{-1}. In both cases, the treatment with 2.2 wt% nitric acid solutions leads to remarkably improved sorption properties in terms of V_t and S_{BET}, which can definitely extract Na^+ cations from the pyrolyzed products with an empirical stoichiometry $C_{(0.4-0.46)} \cdot Na_2O \cdot 2SiO_2$, thereby creating an appreciable volume fraction of voids occupied by constituent Na_2O porogen. Upon acid leaching, the microporosity decreases from 13.7% for Si_py to 10% for Si_py_al, whereas that increases from 13% for Si+B_py to 20.5% for Si+B_py_al. The opposite trend can be explained by the inter-particulate void change that occurs over the course of acid treatment. It is found that acid leaching cannot completely alter the agglomerated properties of the particles derived from the raw polycrystalline Si complex without any B mediator (Figure 7 B) in sharp contrast to the resulting better-divided fine powders from the B-assisted single crystals (Figure 8 B). It is worth noting that acid leaching turns out not to notably modify the mean mesopore widths (Table 2). The large surface area of these silica composites is principally an outcome of very small constituent primary spheres (Figures 7 and 8 insets). The coincident carbon deposits even in significantly low yield are expected to serve as an effective inhibitor minimizing the sintering events to occur on the growing adjacent silica particles during pyrolysis so as to partially offset the adverse effect of sodium silicate binder produced simultaneously, thus contributing to the generation of unwashed silica composites of modest surface area. On the other hand, the resultant silica composites with hierarchical micro-/meso-porosity could inherit to some degree a legacy of porosity from the corresponding layered Si complex precursors. Finally, the atomic arrangement featuring the Si centers free of any direct Si-O-Si linkages (Figure 2) is favorable for the production of high-surface-area silica powders.

Conclusion

In this work, we have utilized a modified transesterification mechanism to solvothermally prepare two well-ordered layered [5]Si complexes with similar crystal phase and empirical formula. Additionally, a novel B-assisted crystallization approach without affecting the elemental kind of the host organosilicate matrix is presented here allowing for the facile preparation of X-ray quality single crystals, whereas no any single crystals but polycrystalline powders are directly attained without the aid of B species as an effective crystal growth modifier. The crystal structure of the B-assisted Si complex with mixed methanolate and glycolate ligands is for the first time determined by SCXRD technique, highlighting the major interlayers intercalated with extensive van der Waals gaps even in the presence of substantial Na^+ counter-ions due to unique atomic arrangement in its crystal structure. The synthetic strategy proposed here offers a generalized route for controllable synthesis of diverse layered metal-organic compounds, which can optionally serve as valuable precursors towards the flexible and facile production of high-surface-area metal oxide composites. Herein, the fabrication of amorphous carbon-silica composites with an appreciable specific surface area is typically exemplified through rapid pyrolysis under inert atmosphere, followed by acid leaching. As such, distinct from the classic sol-gel technique, the present findings afford a new example on how to rapidly synthesize high-surface-area metal oxides. The synthetic methodology of fast pyrolysis is expected to open up a pathway to effectively prepare such functional metal oxides with a broad compositional diversity.

Experimental Section

For general methods of characterization and analysis see the SI.

Synthetic procedures: A distinct transesterification synthetic strategy was created to prepare two layered 5-coordinate organosilicate complexes with different empirical formula. No special care was taken to exclude the exposure to extraneous moisture, and all manipulations were carried out in a well-ventilated fume hood. All chemicals were purchased from Sigma-Aldrich and used as received without further purification.

   Solvothermal synthesis of the B-undoped Si complex: A recipe of $Si(OCH_3)_4$:3EG:$NaOCH_3$:15CH_3OH on a molar basis was originally formulated. In the synthesis, 3.20 g of sodium methoxide powders (97%) were completely dissolved in 18.14 g of anhydrous methanol solvent (99.8%) under intense stirring before the addition of 10.81 g of anhydrous ethylene glycol (EG, 99.8%). After thorough homogenization of the aforementioned solution, 8.91 g of tetramethyl orthosilicate (TMOS, 98%) was rapidly poured into it at room temperature (RT) under agitation.

Subsequently, the highly viscous gel thus formed was transferred into an autoclave, and the solvothermal synthesis was statically carried out at 140 °C under autogenous pressure for 7.5 d. The solid fraction was recovered via vacuum filtration and repeated rinse with copious amounts of anhydrous methanol. The collected solid was vacuum dried at 80 °C for 9 h yielding 8.5 g of dry white polycrystalline powders and then stored in a desiccator for future characterizations.

Solvothermal synthesis of the B-assisted Si complex: To obtain the large single crystals required for crystal structure elucidation, a small fraction of B species was introduced acting as an effective mediator between nucleation and crystal growth. A gel precursor with a molar composition of $0.95Si(OCH_3)_4:0.05B(OCH_3)_3:3EG:NaOCH_3:15CH_3OH$ was prepared by sequentially mixing calculated amounts of anhydrous methanol, $NaOCH_3$, trimethyl borate ($\geq$ 99%), TMOS and EG under intense stirring. The resulting thin gel was aged under stirring overnight at RT. The solvothermal synthesis was statically carried out at 181 °C for 4 d. The solid fraction was collected via vacuum filtration and multiple rinses with plenty of anhydrous methanol. The recovered solid was vacuum dried at 85 °C for 9 h affording 3.3 g of transparent diffraction-quality single crystals, e.g., $0.35 \times 0.20 \times 0.15$ mm^3 in dimension.

Pyrolytic synthesis of porous silica composites: Fast pyrolysis operations were conducted on both of as-synthesized Si complexes in a flowing N_2 atmosphere (25 ml min^{-1}) in a TGA furnace using a ramping rate of 10 °C min^{-1} up to the targeted 800 °C and a soaking time of 8-10 min. In addition, part of these pyrolyzed samples were subsequently rinsed overnight at 50 °C under intense stirring with 2.2 wt% nitric acid aqueous solutions in adequate excess to substantially acid leach the thermally formed Na_2O component. Afterwards, they were collected via vacuum filtration and complete rinse with copious amounts of deionized (DI) water until the pH of the filtrate was neutral, and finally dried at 120 °C overnight for future PXRD, SEM, and N_2 sorption analyses. The resultant samples were denoted as Si_py, Si_py_al, Si+B_py, and Si+B_py_al, where py and al represented pyrolysis and acid leaching treatments, respectively.

[1] R. M. Laine, K. Y. Blohowiak, T. R. Robinson, M. L. Hoppe, P. Nardi, K. Kampf, J. Uhm, *Nature* **1991**, *353*, 642-644.

[2] B. Herreros, S. W. Carr, J. Klinowski, *Science* **1994**, *263*, 1585-1587.

[3] a) K. Y. Blohowiak, D. R. Treadwell, B. L. Mueller, M. L. Hoppe, S. Jouppi, P. Kansal, K. W. Chew, C. L. S. Scotto, F. Babonneau, J. Kampf, R. M. Laine, *Chem. Mater.* **1994**, *6*, 2177-2192; b) P. Kansal, R. M. Laine, *J. Am. Ceram. Soc*. **1994**, *77*, 875-882.

[4] S. D. Kinrade, J. W. D. Nin, A. S. Schach, T. A. Sloan, K. L. Wilson, C. T. G. Knight, *Science* **1999**, *285*, 1542-1545.

[5] A. R. Bassindale, M. Sohail, P. G. Taylor, A. A. Korlyukov, D. E. Arkhipov, *Chem. Commun*. **2010**, *46*, 3274-3276.

[6] a) C. Kobelt, C. Burschka, R. Bertermann, C. F. Guerra, F. M. Bickelhaupt, R. Tacke, *Dalton Trans*. **2012**, *41*, 2148-2162; b) C. Chuit, R. J. P. Corriu, C. Reye, J. C. Young, *Chem. Rev*. **1993**, *93*, 1371-1448.

[7] F. Ma, M. A. Hanna, *Bioresource Techn*. **1999**, *70*, 1-15.

[8] G. J. Gainsford, T. Kemmitt, N. B. Milestone, *Inorg. Chem*. **1995**, *34*, 5244-5251.

[9] S. Qiu, Y. Yu, G. Zhu, O. Terasaki, Y. Nozue, W. Pang, R. Xu, *Micropor. Mesopor. Mater*. **1998**, *21*, 245-251.

[10] T. Kida, K. Kojima, H. Ohnishi, G. Guan, A. Yoshida, *Ceramics International* **2004**, *30*, 727-732.

[11] W. T. Lim, S. M. Seo, T. Okubo, M. Park, *J. Porous Mater.* **2011**, *18*, 305-317.

[12] a) K. Kanamura, C. Zhen, H. Sakaebe, Z. Takehara, *J. Electrochem. Soc*. **1991**, *138*, 331-332; b) G. G. Amatucci, J. M. Tarascon, L. C. Klein, *J. Electrochem. Soc*. **1996**, *143*, 1114-1123; c) G. Che, K. B. Jirage, E. R. Fisher, C. R. Martin, H. Yoneyama, *J. Electrochem. Soc*., **1997**, *144*, 4296-4302.

[13] Y. Wang, Z. Shi, Y. Huang, Y. Ma, C. Wang, M. Chen, Y. Chen, *J. Phys. Chem. C* **2009**, *113*, 13103-13107.

[14] P. Horcajada, T. Chalati, C. Serre, B. Gillet, C. Sebrie, T. Baati, J. F. Eubank, D. Heurtaux, P. Clayette, C. Kreuz, J.-S. Chang, Y. K. Hwang, V. Marsaud, P.-N. Bories, L. Cynober, S. Gil, G. Ferey, P. Couvreur, R. Gref, *Nat. Mater*. **2010**, *9*, 172-178.

[15] Z. Yong, A. E. Rodrigues, *Energy Conversion and Management* **2002**, *43*, 1865-1876.

[16] Z. Xu, J. Fan, S. Zheng, F. Ma, D. Yin, *J. Environ. Qual.* **2009**, *38*, 1302-1310.

[17] a) N. Barrabes, D. Cornado, K. Föttinger, A. Dafinov, J. Llorca, F. Medina, G. Rupprechter, *J. Catal.* **2009**, *263*, 239-246; b) M. Chhowalla, H. S. Shin, G. Eda, L.-J. Li, K. P. Loh, H. Zhang, *Nat. Chem*. **2013**, *5*, 263-275.

[18] Y. Z. Chen, C. M. Hwang, C. W. Liaw, *Appl. Catal. A: General* **1998**, *169*, 207-214.

[19] A. D. Irwin, J. S. Holmgren, T. W. Zerda, J. Jonas, *J. Non-Cryst. Solids* **1987**, *89*, 191-205.

[20] R. Bandyopadhyay, Y. Kubota, N. Sugimoto, Y. Fukushima, Y. Sugi, *Micropor. Mesopor. Mater.* **1999**, *32*, 81-91.

[21] S. I. Zones, S.-J. Hwang, *Micropor. Mesopor. Mater.* **2011**, *146*, 48-56.

[22] R. J. Hill, G. V. Gibbs, *Acta Crystallogr. Sec. B-Struct. Sci.* **1979**, *35*, 25-30.

[23] J. B. Parise, T. E. Gier, *Int. J. Inorg. Mater.* **2000**, *2*, 81-86.

[24] X. Li, V. K. Michaelis, T.-C. Ong, S. J. Smith, I. McKay, P. Müller, R. G. Griffin, E. N. Wang, *CrystEngComm.* **2014**, *16*, 2950-2958.

[25] K. C. Kumara Swamy, V. Chandrasekhar, J. J. Harland, J. M. Holmes, R. O. Day, R. R. Holmes, *J. Am. Chem. Soc*. **1990**, *112*, 2341-2348.

[26] W. H. Baur, *Acta Crystallogr. Sec. B-Struct. Sci.* **1978**, 34, 1751-1756.

[27] R. T. Downs, G. V. Gibbs, K. L. Bartelmehs, M. B. Boisen, *Am. Mineralogist* **1992**, *77*, 751-757.

[28] A. J. Lussier, P. M. Aguiar, V. K. Michaelis, S. Kroeker, F. C. Hawthorne, *Am. Mineralogist* **2009**, *94*, 785-792.

[29] A. J. Lussier, F. C. Hawthorne, V. K. Michaelis, P. M. Aguiar, S. Kroeker, *Periodico di Mineralogia* **2011**, *80*, 57-73.

[30] T. Oh, C. K. Choi, *J. Korean Phys. Soc.* **2010**, *56*, 1150-1155.

[31] F. Gan, *Optical and spectroscopic properties of glass*, Springer-Verlag, Berlin, **1992**.

[32] CCDC-965918 contains the supplementary crystallographic data for this paper.

Entry for the Table of Contents

Transesterification

Xiansen Li,* Vladimir K. Michaelis, Ta-Chung Ong, Stacey J. Smith, Robert G. Griffin, Evelyn N. Wang*

Designed Single-Step Synthesis, Structure, and Derivative Textural Properties of Well-Ordered Layered Penta-Coordinate Silicon Alcoholate Complexes
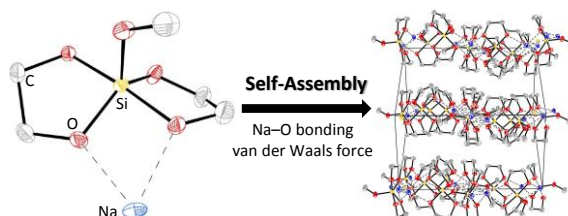
van der Waals gap! Well-ordered layered penta-coordinate silicon alcoholate is prepared via a new single-step transesterification mechanism, whose structure is elucidated with one single crystal directly acquired by a novel boron-mediated synthetic route; these complexes are very effective precursors for the facile preparation of high-surface-area amorphous silica powders.
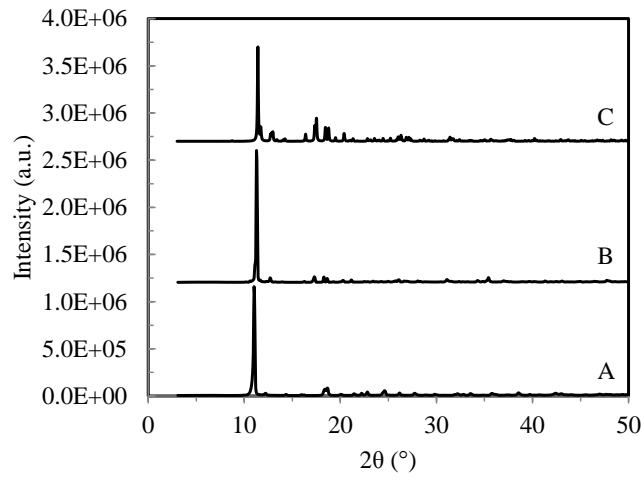
Figure 1. Experimental PXRD patterns of as-prepared B-undoped Si complex polycrystalline powders (A) and numerous B-assisted Si complex single-crystals (B), and simulated pattern of one single crystal of the B-assisted Si complex (C).
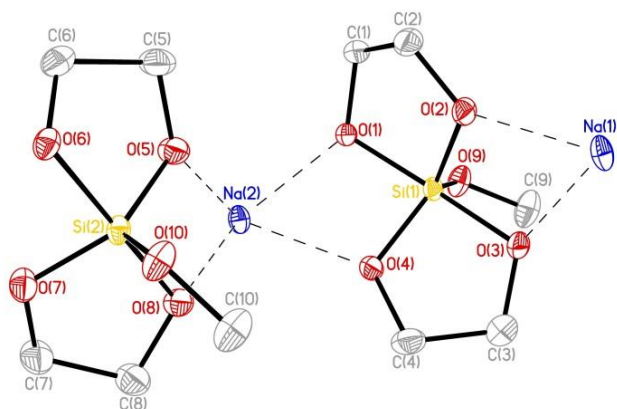
Figure 2. Asymmetric unit of the B-assisted crystal structure showing the sodium tetrakis(glycolato)bis(methanolato)silicate complex $Na_2Si_2(OCH_3)_2(OCH_2CH_2O)_4$.[55] C5 and C6 positional disorders, and hydrogen atoms are omitted for clarity, and thermal ellipsoids are set to 50% probability.
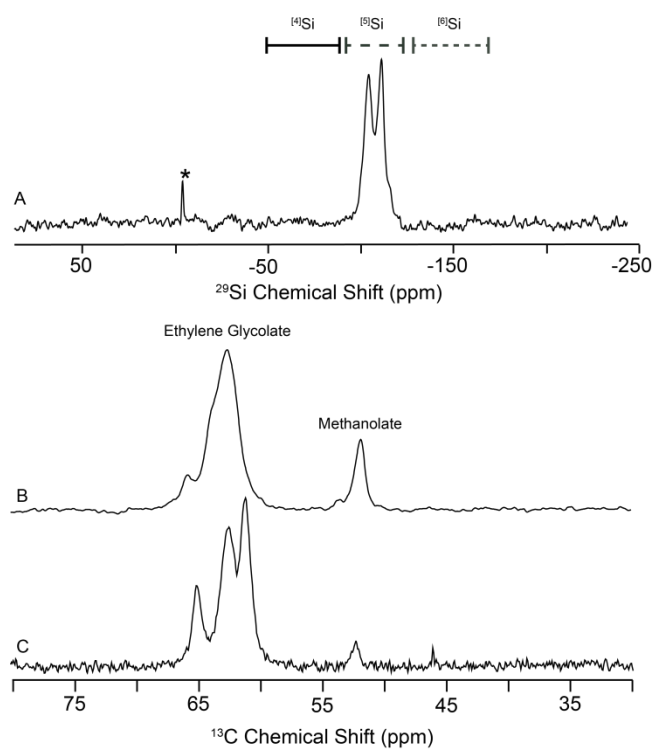
Figure 3. MAS NMR of the Si complexes at 16.4 T (697 MHz, ^{1}H): both ^{29}Si (A) and ^{13}C (B) of B-assisted complex as well as ^{13}C of B-undoped one (C). *transmitter offset.
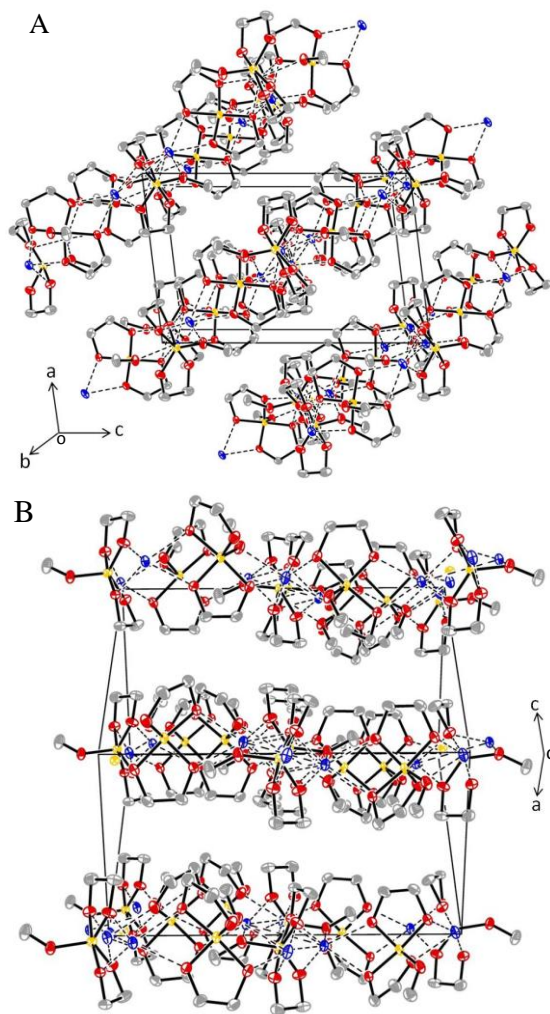
Figure 4. Packing plots of the B-assisted Si complex viewed along the crystallographic *b* axis (A) and [101] direction (B). Hydrogen atoms are omitted for clarity. Blue: Na; Red: O; Gray: C; and Yellow: Si.
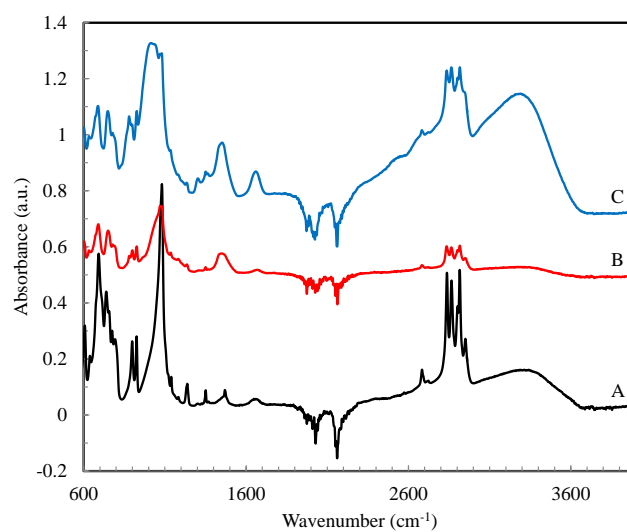
Figure 5. ATR-FTIR spectra of the B-undoped Si complex (A), and the B-assisted one without (B) and with (C) exposure to ambient air for 10 min.
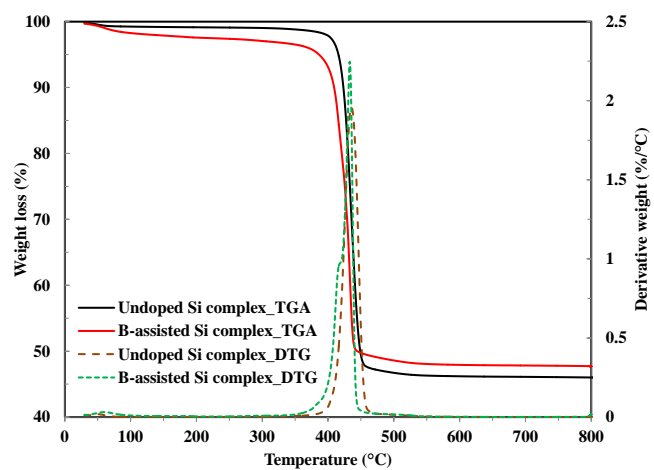
Figure 6. TG and DTG (derivative thermogravimetry) profiles for the B-assisted and B-undoped Si complexes running in flowing N_2 atmospheres.
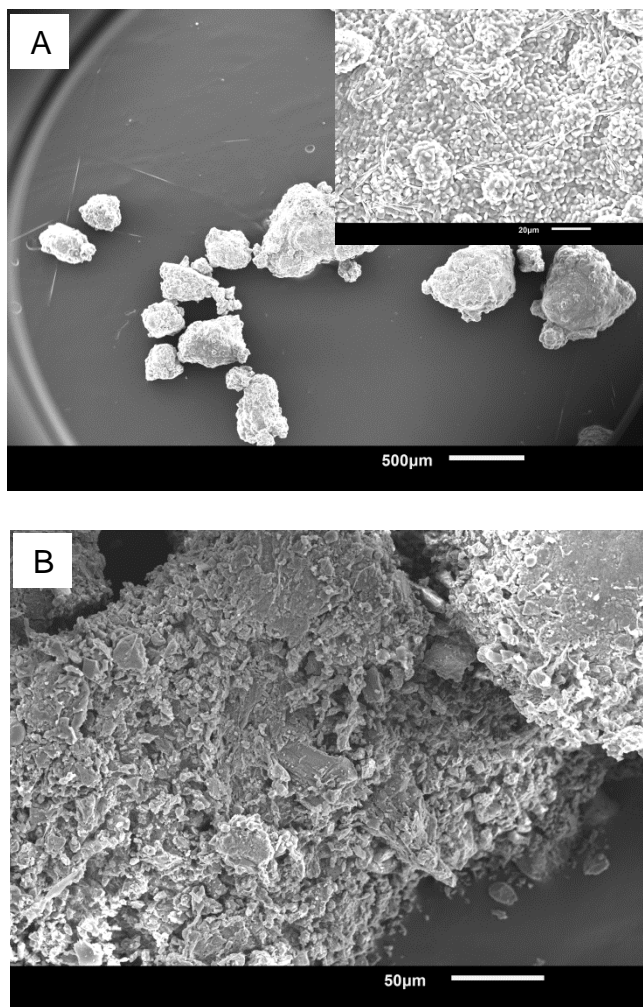
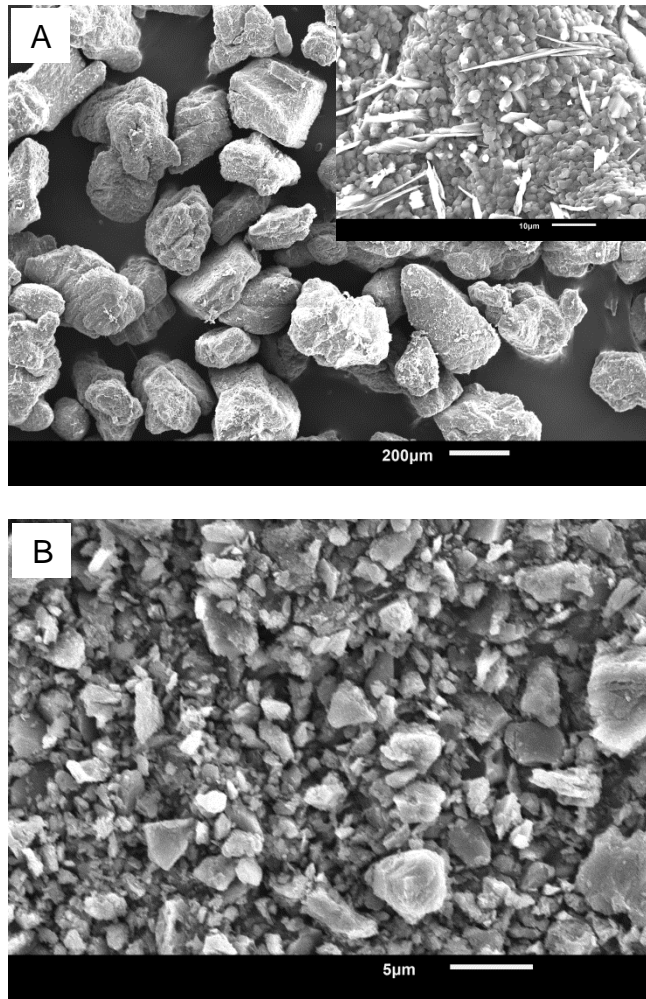Figure 7. SEM images of Si_py (A) and Si_py_al (B), and an enlarged image of Si_py in the inset.

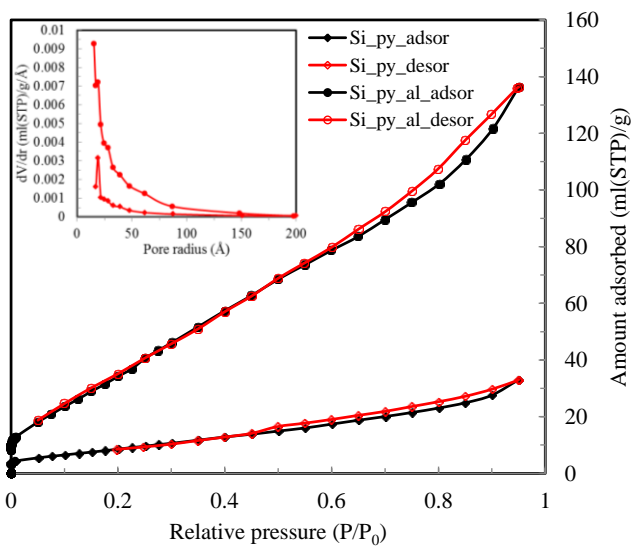**Figure 8. SEM images of Si+B_py (A) and Si+B_py_al (B), and an enlarged image of Si+B_py in the inset.**

Figure 9. N$_2$ adsorption/desorption isotherms of Si_py and Si_py_al, and their corresponding PSDs in the inset (Si_py: ♦, and Si_py_al: ●).
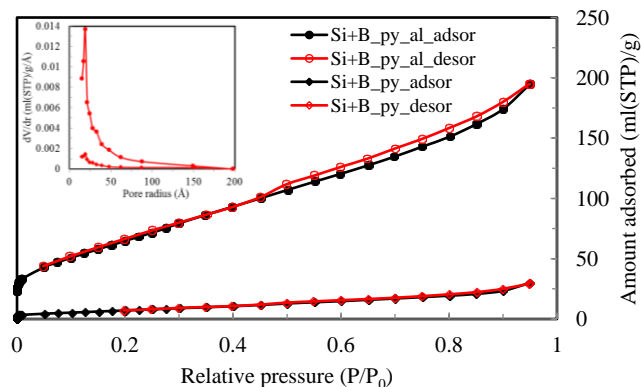
Figure 10. N$_2$ adsorption/desorption isotherms of Si+B_py and Si+B_py_al, and their corresponding PSDs in the inset (Si+B_py: ♦, and Si+B_py_al: ●).

Tables:

Table 1. Elemental analytical and SCXRD-derived results for both Si complexes with and without B mediator (wt%).

Entry	Formula	Source	B	C	H	Na	Si
w/o boron	Na$_{1.94}$Si$_2$C$_{9.80}$H$_{21.44}$O$_{10.82}$ [a]	Expt.	---	28.46±0.028	5.24±0.021	10.80±0.023	13.60±1.8
w/ boron	Na$_{1.90}$Si$_2$C$_{8.18}$H$_{19.11}$O$_{10.30}$ [a]	Expt.	< 0.96	25.70±0.48	5.05±0.13	11.40±0.03	14.70±2.5
	Na$_2$Si$_2$C$_{10}$H$_{22}$O$_{10}$	SCXRD	0.00	29.67	5.49	11.37	13.89

[a] Oxygen content is obtained by difference, and the potential effect of surface carbonate species on carbon quantity is ignored.

Table 2. Textural parameters for the pyrolyzed samples with and without acid leaching.

Sample	V_t (ml g^{-1})	V_{meso} (ml g^{-1})	V_{micro} (ml g^{-1})	S_{BET} (m^2 g^{-1})	d_{meso} at max. PSD (nm)
Si_py	0.051±0.013	0.044±0.014	0.007±0.004	35.5±1.1	3.82
Si_py_al	0.211±0.033	0.19±0.033	0.021±0.002	163.3±22	3.06
Si+B_py	0.046±0.007	0.040±0.007	0.006±0.002	30.0±1.6	3.84
Si+B_py_al	0.302±0.023	0.24±0.023	0.062±0.002	254.7±8.2	3.83

Supporting Information

Designed Single-Step Synthesis, Structure, and Derivative Textural Properties of Well-Ordered Layered Penta-Coordinate Silicon Alcoholate Complexes

Xiansen Li,[*][a] Vladimir K. Michaelis,[b,c] Ta-Chung Ong,[b,c] Stacey J. Smith,[b] Robert G. Griffin,[b,c] and Evelyn N. Wang[*][a]

[a]Department of Mechanical Engineering, [b]Department of Chemistry and [c]Francis Bitter Magnet Laboratory, Massachusetts Institute of Technology, Cambridge, Massachusetts 02139, USA

[*] To whom correspondence should be addressed.

E-mail: xsli@mit.edu (X. Li) and enwang@mit.edu (E. Wang).

1. Methods of characterization

1.1. PXRD: PXRD pattern was taken on the Si complexes and pyrolyzed Si complexes without dilute acid leaching using a PANalytical X'Pert Pro Multipurpose Diffractometer in reflectance Bragg-Brentano geometry at 45 kV and 40 mA under Ni-filtered Cu $K\alpha$ radiation ($\lambda = 1.5418$ Å). The data collection was carried out at a constant temperature of 25 °C with a step increment of 0.084° 2θ, a counting time of 6.4 s/step, and the 2θ angular range from 3 to 50°.

 The simulated PXRD pattern of the B-assisted Si complex was based on the .cif file containing the structural parameters (unit cell size, space group symmetry, and atomic coordinates, *etc.*) from the refined SCXRD structure that was imported into a software package-Mercury 3.1 which then used these structural parameters to calculate what the PXRD pattern should look like.

1.2. SCXRD: Low-temperature (-173 °C) XRD data comprising φ- and ω-scans were collected using a Bruker-AXS X8 Kappa Duo diffractometer coupled to a Smart Apex II CCD detector with an *IμS* source of Mo $K\alpha$ radiation ($\lambda = 0.71073$ Å). The structure was solved by direct methods using SHELXS[1] and refined against F^2 on all data by full-matrix least squares with SHELXL-97[2] using established refinement strategies.[3] All non-hydrogen atoms were refined anisotropically. The positions of all hydrogen atoms were calculated geometrically and refined using a riding model. The isotropic displacement parameters of all hydrogen atoms were fixed to be 1.2 times the Ueq value of the atom to which they were bound (1.5 for methyl groups). The carbon atoms (C5 and C6) of one of the ethylene glycolate chelators on Si2 are disordered over two positions (omitted for clarity in Figure 2). Similarity restraints are used for the 1-2 and 1-3 distances for these atoms, and their displacement parameters are constrained to be equal. Rigid bond and similarity restraints are employed on the displacement parameters for both glycolates on Si1.

1.3. MAS NMR spectroscopy: Solid-state NMR experiments were performed using either a 9.4 (400 MHz, ^{1}H), 11.7 (500 MHz, ^{1}H), or 16.4 T (697 MHz, ^{1}H) magnet, each equipped with a home-built NMR spectrometer (courtesy of Dr. D. Ruben, FBML-MIT). Spectra were acquired using a series of NMR probes including a 3.2 mm home-built double resonance ([1]H-X, X = [29]Si), a 3.2 mm Chemagnetics triple-resonance (^{1}H/^{13}C/^{15}N), or a triple-resonance (^{1}H/X/Y, X = [11]B or [29]Si) MAS probe for [11]B, ^{13}C, and [29]Si. The white crystalline sample was ground using an agate mortar and pestle under dry N_2 gas and packed into a 3.2 mm (o.d.) high-volume thin-wall ZrO_2 rotor (~34 μl fill volume). The magic angle within the probe was set using the [79]Br resonance of solid KBr and shimmed using adamantane prior to signal acquisition. Sample temperatures were regulated between 22 and 26 °C during acquisition. All spectra were processed using RNMRP data processing software (courtesy of Dr. D. Ruben, FMBL-MIT).

 ^{29}Si MAS NMR spectra (9.4 and 16.4 T, $\omega_L/2\pi = 78$ and 138 MHz, [29]Si $\chi B_1/2\pi = 50$ kHz) were acquired using either a Bloch or Hahn-echo[4] and a spinning frequency between 10,000 and 11,500(3) Hz, 1,536 and 8,196 co-added transients, and a recycle delay of 60 s, respectively. All data were acquired with high-power ([1]H $\chi B_1/2\pi = 83$ kHz) two-pulse phase modulation (TPPM) ^{1}H decoupling during acquisition. [29]Si spectra were referenced with respect to neat TMS (0 ppm).[5]

 ^{13}C MAS NMR spectra (11.7 and 16.4 T, $\omega_L/2\pi = 126$ and 175 MHz) were acquired using [13]C{[1]H} CP[6] at a $\omega_r/2\pi = 13,500(3)$ Hz, 16,384 co-added transients and a recycle delay of 4 s, respectively. The contact time during the CP experiment was set to 1.5 ms and acquired using high-power ([1]H $\chi B_1/2\pi = 83$ kHz) TPPM[7] [1]H decoupling during acquisition. [13]C spectra were referenced relative to solid adamantane at 40.49 ppm (high frequency resonance).[8]

 ^{11}B MAS NMR spectra (16.4 T, $\omega_L/2\pi = 223$ MHz) were acquired using a Bloch[9] experiment with a short quantitative tip angle (15°, [11]B $\chi B_1/2\pi = 50$ kHz), a spinning frequency, $\omega_r/2\pi = 16,500(4)$ Hz, and a series of varying recycle delays (between 3 and 15 s) and co-added

transients (between 8,196 and 98,304). [11]B spectra were referenced relative to 0.1 M H_3BO_3 solution at 19.6 ppm with respect to BF_3-Et_2O (0 ppm).[10]

1.4. ATR-FTIR spectroscopy: IR absorbance spectra were collected using a Nexus 870 FT-IR E.S.P. spectrometer (Thermo Scientific) equipped with an ATR accessory with a single reflection diamond crystal. The FT-IR chamber was flushed constantly with N_2 (*ca.* 0.71 m^3 h^{-1}). Prior to data collection, the chamber was purged with flowing N_2 stream for at least 15 min. Scans at a spectral resolution of ± 4 cm^{-1} were taken at RT on a self-supporting sample disc from 600 to 4000 cm^{-1}. Sixteen scans were averaged, and the resulting spectra were background subtracted.

1.5. Elemental analysis: For bulk elemental analysis, the samples were sent to Galbraith Laboratories, Knoxville, TN. They were dried at 70 °C for 4 h in vacuo before quantifying carbon and hydrogen elements. Elemental analyses were performed for silicon, sodium, and boron as well. The content of oxygen was obtained by difference.

1.6. TG analysis: The sample of Si complex with an initial mass of several tens of mg was heated in a Pt pyrolytic pan at a constant ramping rate of 10 °C min^{-1} from ambient temperature up to 800 °C on a Discovery TG analyzer from TA Instruments in a flowing N_2 atmosphere preset to 25 ml min^{-1}. The isothermal duration at 800 °C was set to 3 min. The experimental corrected sample standard deviations in TGA analyses were 0.034% and 0.18% for the B-assisted and B-undoped Si complexes, respectively.

1.7. SEM: The morphology of the pyrolyzed silica particles before and after dilute acid rinses was characterized by an Analytical Scanning Electron Microscope (JEOL-6010LA) at an accelerating voltage of 10 or 15 kV. A gold film was sputter-coated onto these samples before imaging.

1.8. Gas sorption analysis: Gas sorption studies were conducted to investigate the textural properties of the pyrolyzed products with and without a dilute acid leaching treatment. The N_2 sorption measurements were performed at -196 °C using an Autosorb iQ_2 automated gas sorption analyzer (Quantachrome). Before adsorption runs, each sample was degassed under vacuum (*ca.* 0.2 Pa) at 370 °C for 12 h, and a proper glass rod filler was then inserted in the corresponding sample cell to minimize the cell dead void. The BET (Brunauer, Emmett, and Teller) surface area, S_{BET}, was obtained by applying the BET equation to a relative pressure (RP) range of 0.05-0.30 on the adsorption branch. The total pore volume, V_t, was evaluated from the adsorbed N_2 amount at a maximal RP of 0.95. The micropore volume, V_{micro}, was determined by applying the D-R (Dubinin-Radushkevich) equation to a RP range of 0.0003-0.009 on the adsorption isotherm. The pore size distribution (PSD) was calculated by the BJH (Barrett, Joyner, and Halenda) method on the desorption branch.

2. Experimental Results

Table S1. Crystal data and structure refinement for the B-assisted Si complex.

Parameter	Data
Identification CCDC No.	965918
Empirical formula	$C_{10}H_{22}Na_2O_{10}Si_2$
Formula weight	404.44
Temperature	100(2) K
Wavelength	0.71073 Å
Crystal system	Monoclinic
Space group	P2(1)/n

|		
	$a = 8.7279(5)$ Å	$\alpha = 90°$
Unit cell dimension	$b = 15.0981(9)$ Å	$\beta = 96.8920(10)°$
	$c = 13.7362(9)$ Å	$\gamma = 90°$
Volume	$1797.00(19)$ Å^3	
Z	4	
Density (calculated)	1.495 Mg m^{-3}	
Absorption coefficient	0.291 mm^{-1}	
$F(000)$	848	
Crystal size	$0.35 \times 0.20 \times 0.15$ mm^3	
Theta range for data collection	2.01 to 31.50°	
Index ranges	$-12 \le h \le 12$, $-22 \le k \le 20$, $-20 \le l \le 20$	
Reflections collected	54664	
Independent reflections	5975 [$R(int) = 0.0306$]	
Completeness to theta = 31.50°	100.0 %	
Absorption correction	Semi-empirical from equivalents	
Max. and min. transmission	0.9577 and 0.9051	
Refinement method	Full-matrix least-squares on F^2	
Data/restraints/parameters	5975/112/226	
Goodness-of-fit on F^2	1.067	
Final R indices [$I > 2\sigma(I)$]	$R1 = 0.0370$, $wR2 = 0.1050$	
R indices (all data)	$R1 = 0.0428$, $wR2 = 0.1093$	
Largest diff. peak and hole	1.364 and -0.587 e Å^{-3}	
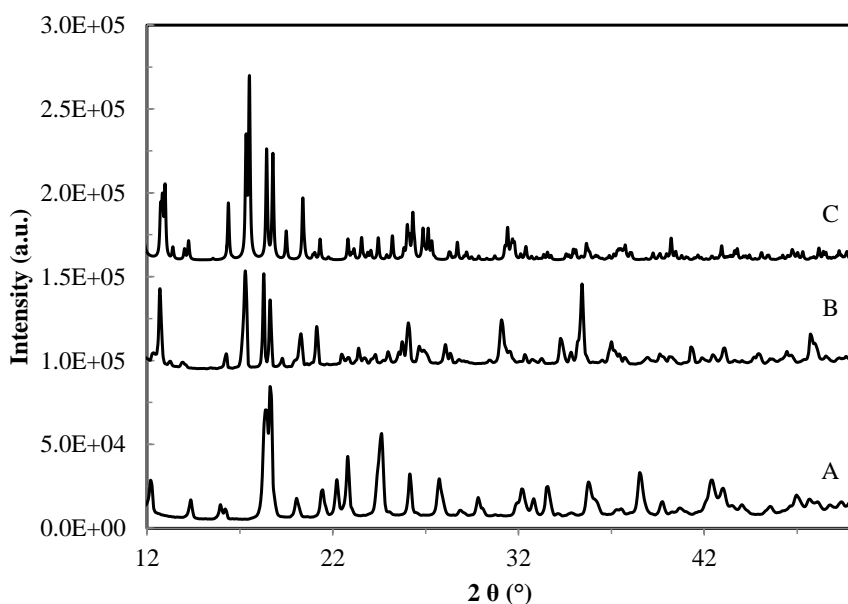
Figure S1. Experimental PXRD patterns of as-prepared B-undoped Si complex polycrystalline powders (A) and numerous B-assisted Si complex single-crystals (B), and simulated PXRD pattern from single-crystal X-ray data of the B-assisted Si complex (C). Three XRD patterns are all magnified in the high-angle region.

3. References

[1] G. M. Sheldrick, *Acta Cryst.* **1990**, *A46*, 467-473.
[2] G. M. Sheldrick, *Acta Cryst.* **2008**, *A64*, 112-122.
[3] P. Müller, *Crystallography Reviews* **2009**, *15*, 57-83.
[4] E. L. Hahn, *Phys. Rev.* **1950**, 80, 580-594.
[5] R. K. Harris, E. D. Becker, *J. Magn. Reson.* **2002**, *156*, 323-326.
[6] A. Pines, J. S. Waugh, M. G. Gibby, *J. Chem. Phys.* **1972**, *56*, 1776-1777.

[7] A. E. Bennett, C. M. Rienstra, M. Auger, K. V. Lakshmi, R. G. Griffin, *J. Chem. Phys.* **1995**, *103*, 6951-6958.

[8] C. R. Morcombe, K. W. Zilm, *J. Magn. Reson.* **2003**, *162*, 479-486.

[9] F. Bloch, *Phys. Rev.* **1946,** *70*, 460-475.

[10] R. K. Harris, E. D. Becker, *J. Magn. Reson.* **2002**, *156*, 323-327.